Biochimica et Biophysica Acta 1797 (2010) 457–465

Contents lists available at ScienceDirect

Biochimica et Biophysica Acta

journal homepage: www.elsevier.com/locate/bbabio

The molecular structure of the IsiA–Photosystem I supercomplex, modelled from high-resolution, crystal structures of Photosystem I and the CP43 protein

Yinan Zhang [a,b,c,d], Min Chen [a], W. Bret Church [e], Kwok Wai Lau [a,b,f], Anthony W.D. Larkum [a,b], Lars S. Jermiin [a,b,g,h,i,*]

[a] School of Biological Sciences, University of Sydney, Sydney, NSW 2006, Australia
[b] Sydney Bioinformatics, University of Sydney, Sydney, NSW 2006, Australia
[c] School of Information Technologies, University of Sydney, Sydney, NSW 2006, Australia
[d] School of Pharmacy, Shanghai Jiao Tong University, Shanghai 200240, People's Republic of China
[e] Faculty of Pharmacy, University of Sydney, Sydney, NSW 2006, Australia
[f] Division of Mathematics, Informatics and Statistics, CSIRO, Wembley, WA 6913, Australia
[g] Centre for Mathematical Biology, University of Sydney, Sydney, NSW 2006, Australia
[h] Division of Entomology, CSIRO, Canberra, ACT 2601, Australia
[i] Department of Biochemical Sciences "Rossi Fanelli", University of Rome, "Sapienza", 00185 Rome, Italy

ARTICLE INFO

Article history:
Received 12 November 2009
Received in revised form 31 December 2009
Accepted 5 January 2010
Available online 11 January 2010

Keywords:
IsiA–PSI supercomplex
Chlorophyll
Molecular modelling
Multi-objective optimization
Energy-transfer potential
Photosynthesis

ABSTRACT

We present the molecular structure of the IsiA–Photosystem I (PSI) supercomplex, inferred from high-resolution, crystal structures of PSI and the CP43 protein. The structure of iron-stress-induced A protein (IsiA) is similar to that of CP43, albeit with the difference that IsiA is associated with 15 chlorophylls (Chls), one more than previously assumed. The membrane-spanning helices of IsiA contain hydrophilic residues many of which bind Chl. The optimal structure of the IsiA–PSI supercomplex was inferred by systematically rearranging the IsiA monomers and PSI trimer in relation to each other. For each of the 6,969,600 structural configurations considered, we counted the number of optimal Chl–Chl connections (i.e., cases where Chl-bound Mg atoms are $\leq$25 Å apart). Fifty of these configurations were found to have optimal energy-transfer potential. The 50 configurations could be divided into three variants; one of these, comprising 36 similar configurations, was found to be superior to the other configurations in terms of its potential to transfer excitation energy to the reaction centres under low-light conditions and its potential to dissipate excess energy under high-light conditions. Compared to the assumed model [Biochemistry 42 (2003) 3180–3188], the new Chl increases by 7% the ability of IsiA to harvest sunlight while the rearrangement of the constituent components of the IsiA–PSI supercomplex increases by 228% the energy-transfer potential. In conclusion, our model allows us to explain how the IsiA–PSI supercomplex may act as an efficient light-harvesting structure under low-light conditions and as an efficient dissipater of excess energy under high-light conditions.

1. Introduction

The photosynthetic machinery in oxygenic photosynthetic organisms comprises two types of light-harvesting (LH) protein complexes [1]. In 'classical' cyanobacteria and some algae (i.e., Rhodophyta, Glaucophyta, and Cryptophyta), the primary LH system is a membrane-extrinsic, phycobilin-binding protein (PBP) complex. In all other groups of oxygenic photosynthetic organisms (i.e., other algae and plants), the primary LH system is a membrane-intrinsic, chlorophyll (Chl)-binding protein (CBP) complex.

The iron-stress-induced A protein (IsiA) is an important LH molecule in cyanobacteria. In its natural form, IsiA binds Chl and acts as an accessory antenna protein [2]. In most 'classical' cyanobacteria, where Chl *a* is the only Chl available, IsiA is expressed under iron deprivation, when photosystems I and II (PSI and PSII) and the phycobilisomes (PBS) are down-regulated, and the number of Chls in the cell is increased [3,4]. Expression of IsiA has also been observed in cyanobacteria that live in oxygenated environments or grow under intense light [5,6], and it has been suggested that IsiA protects cyanobacteria from photo-oxidative stress through a dissipative process [7,8]. Up-regulated transcription of the IsiA gene has been observed in mutants of *Synechocystis* sp. PCC 6803, such as the cytochrome c_6-deficient mutant [9] and the psaFJ-null mutant [10]. Expression of IsiA appears to be regulated at both transcriptional and post-transcriptional levels [11,12]. An IsiA-like protein, the prochlorophyte Chl-binding protein (Pcb), is expressed both constitutively and inducibly (by low iron conditions) in *Prochlorococcus* [13] and constitutively in *Acaryochloris marina* [2].

* Corresponding author. CSIRO Entomology, GPO Box 1700, Canberra, ACT 2601, Australia. Tel.: +61 2 6246 4043; fax: +61 2 6246 4094.
E-mail address: lars.jermiin@csiro.au (L.S. Jermiin).

0005-2728/$ – see front matter © 2010 Elsevier B.V. All rights reserved.
doi:10.1016/j.bbabio.2010.01.002

Based on electron microscopy studies of the IsiA–PSI supercomplex, a polymer of 18 IsiA molecules has been found to encircle the PSI trimer in *Synechocystis* sp. PCC 6803 [14,15]. The IsiA–PSI supercomplex appears to be stable [16] and to provide efficient transfer of energy between the IsiA ring and the PSI trimer [17,18]. Nield et al. [19] modelled the structure of the IsiA–PSI supercomplex. The structure of their model of the PSI trimer was modelled on the basis of a high-resolution (2.5 Å) crystal structure of PSI [20] while that of their IsiA ring was modelled on the basis of a low-resolution (3.8 Å) crystal structure of CP43 [21], an antenna protein of PSII that is homologous with IsiA [22,23]. Twelve Chls, found to be associated with CP43 in the crystal structure of PSII [21], were included in Nield et al.'s [19] model of the IsiA–PSI supercomplex. Other studies have shown that 13 or 14 Chls may be associated with CP43 [24–26]. Thus, the number and positions of Chls associated with IsiA remain uncertain.

Recent research has revealed that IsiA can form other polymeric structures. For example, it was found to form a 17-mer ring around the PSI trimer in *Synechocystis* sp. PCC6803 when the PsaF and PsaJ proteins are missing [27]. It has also been shown that more than one ring of IsiA monomers can occur [28]. Other reports suggest that IsiA is not always found in association with the PSI trimer. For example, Aspinwall et al. [29] found that six or seven monomers of IsiA occasionally may connect to a PSI monomer whereas Yeremenko et al. [30] reported that IsiA monomers can form empty rings, which may be responsible for thermal energy dissipation [31]. What initiates and stabilizes the connections between the IsiA ring and the PSI trimer are unresolved questions.

In addition to its known role as an antenna protein in PSI [14,32], IsiA has been found to act as a photo-inhibitor for PSII [33]; however, this aspect of its role will not be addressed here, partly because structural information on the IsiA–PSII supercomplex is not yet available.

Here, we present and compare molecular structures of IsiA, the IsiA ring, and the IsiA–PSI supercomplex. These molecular structures were inferred using as templates high-resolution crystal structures of PSI (at 2.5 Å [20]), which includes the PsaA, PsaB, and PsaJ proteins, and CP43 (at 3.0 Å [34] and 3.5 Å [25]). The positions of Chls and carotenoids associated with IsiA were determined. Functionally optimal structures of the IsiA–PSI supercomplex were determined using results obtained from *Cartesian*, a new program to manipulate and calculate distances between atoms in the IsiA–PSI supercomplex. Optimal configurations of the IsiA–PSI supercomplex (defined below) were identified from a total of 6,969,600 structural configurations. Based on the coordinates of Chls in these optimal configurations of the IsiA–PSI supercomplex, we then identified those Chls that may be most critical in terms of transferring energy between the IsiA monomers and between the IsiA ring and the PSI trimer.

2. Materials and methods

The models constructed here were based on those of Bibby et al. [16] and Nield et al. [19]. Since there are 18 IsiA monomers in the ring that surrounds the PSI trimer, each IsiA monomer must cover 20° of the IsiA–PSI supercomplex and have a 20° inclination compared to its neighbours. Hence, denoting the radii of the PSI trimer and IsiA as R and r, in the plane of the membrane, we can estimate these radii from the radius of the IsiA–PSI supercomplex (S) using the following formula:

$$S = R + 2r \tag{1}$$

where

$$r = \frac{R \sin 10^{\circ}}{1 - \sin 10^{\circ}}. \tag{2}$$

Given that $S = 160$ Å [19], we obtain $R = 112$ Å and $r = 24$ Å.

IsiA was modelled using *SWISS-MODEL* version 3.5 [35] with CP43 as a template (1S5L and 2AXT from Protein Data Bank [36]). The positions of the Chl-binding amino acids associated with IsiA were first modelled on the basis of 14 CP43-associated Chls [25], which accords with literature on the subject [19]. Given the three-dimensional structures of IsiA, CP43, and the N-terminal sequences of PsaA and PsaB (i.e., the first six helices and five loops), which are homologous proteins [23], we inferred a multiple sequence alignment for the amino-acid sequences of IsiA, CP43, CP47, PsaA, and PsaB (relevant details are included in the Supplementary Material). Using this alignment, we discovered an extra conserved histidine in IsiA (H159), which is homologous to conserved Chl-binding histidines in PsaA and PsaB. As Chl may bind to this histidine, we modelled the structure of IsiA under the assumption that IsiA is associated with an additional Chl, which binds to the H159 residue.

The inferred structure of IsiA was validated using *ValPred*, a program that implements a method described in Dastmalchi et al. [37], and *Harmony* [38], a program that is similar to *ValPred*, except that it also uses a sequence with the amino acids in reverse order (as a control). Based on its biochemical properties, both programs produce a compatibility score for each amino acid with zero indicating an intermediate state of reliability, lower scores representing regions of lower reliability, and higher scores representing higher reliability. Compatibility with the membrane environment is also considered in the implementation of *ValPred*.

We examined the sequences of amino acids in the six membrane-spanning helices of IsiA to determine whether there were any unexpected properties associated with these helices (e.g., the presence of strongly hydrophilic amino acids). For each of these helices, we estimated the average hydropathy score using the hydropathy indices of Kyte and Doolittle [39]. The relevant residues for this part of the study were 40–67, 105–127, 150–173, 216–238, 254–276 and 317–343 in IsiA from *Thermosynechococcus elongatus* [40].

The number and locations of optimal Chl–Chl connections (i.e., connections that support efficient transfer of energy between adjacent Chls) within and between subsections of the IsiA–PSI supercomplex were identified using *Cartesian*, a program that allowed us (*i*) to rearrange the IsiA monomers, the ring of IsiA, and the PSI trimer in relation to each other, and (*ii*) calculate Euclidean distances between Chls in the IsiA–PSI supercomplex (written by LSJ; included in the Supplementary Material). According to quantum field theory, Förster's [41] transition rate is proportional to D^{-6} when the radiator and acceptor molecules are separated by a distance, D, which, in this study, is that between two Mg atoms in adjacent Chls. Hence, we define an optimal Chl–Chl connection as occurring when Chl-bound Mg atoms are ≤ 25 Å apart [42]. This distance is consistent with those reported previously [18,43,44].

To further examine the position of IsiA monomers within the thylakoid membrane, we used *Swiss-PdbViewer* version 3.7 [35] and *Cartesian* to compare configurations of: (*i*) the lumen model, in which the 5th loop of each IsiA monomer faced the thylakoid lumen; and (*ii*) the stroma model, in which the 5th loop of each IsiA monomer faced the stroma. The approach used to obtain and compare different configurations of the IsiA–PSI supercomplex was as follows:

1. The IsiA–PSI supercomplex was constructed using *PyMOL* version 0.99 [45] and a script written by K Castle (available on request). The centroid of the PSI trimer (1JB0 from Protein Data Bank [36]) was chosen as the centre of the supercomplex, after which a ring of 18 IsiA monomers, each with 15 Chls, was added so that: (*i*) the periphery of this ring matches that of the IsiA–PSI supercomplex, (*ii*) the centroids of the IsiA ring and the PSI trimer overlap, (*iii*) the 5th loop of each IsiA monomer faces the thylakoid lumen, and

(*iv*) Helices V and VI of each IsiA monomer face the PSI trimer. This model is similar to that of Nield et al. [19], which was based on crystal structures of CP43 in PSII [25,34]. The symmetry of this model, henceforth called the Reference model, was confirmed using *Cartesian*. The 288 Chls associated with the PSI trimer were assumed to occupy the same positions as those in Nield et al.'s [19] model.

2. The Reference model was then modified by, independently, (*i*) moving the PSI trimer along its major axis in steps of 0.5 Å from −30 Å to +30 Å; (*ii*) rotating the PSI trimer around its major axis in steps of 0.5° from 0° to 20°; and (*iii*) simultaneously rotating the 18 IsiA monomers around their own axes in steps of 0.5° from 0° to 360°.
3. The numbers of optimal Chl–Chl connections (i.e., Chl-bound Mg atoms that are ≤25 Å) between adjacent IsiA monomers, d_1, and between the IsiA ring and PSI trimer, d_2, were recorded for 3,484,800 configurations.
4. In order to consider the same number of stroma-model configurations, we modified the Reference model by flipping the IsiA ring 180°, after which we repeated the preceding two steps.
5. The resulting 6,969,600 configurations of the IsiA–PSI supercomplex were compared in a two-dimensional Pareto plot [46]. For each configuration, we calculated the joint energy-transfer potential (defined as the sum of optimal Chl–Chl connections (*i*) between adjacent IsiA monomers and (*ii*) between the IsiA ring and the PSI trimer). Configurations with the highest joint energy-transfer potential were selected as optimal models of the IsiA–PSI supercomplex.

We finally wished to examine the anti-parallel model, in which the 5th loop of adjacent IsiA monomers faced the lumen and stroma alternatively, but our study of the arrangement of the six membrane-spanning helices of IsiA led us to conclude that the anti-parallel model was unlikely to exist (see below).

3. Results

IsiA was modelled on the basis of the known structure of CP43. According to our model, IsiA is associated with 15 Chls, 14 of which are in similar positions to matching Chls in CP43 and the N-terminal segments PsaA and PsaB. By comparing the structure of IsiA to those of PsaA and PsaB, each of which is associated with an additional 12 Chls, we found that IsiA has one additional histidine, H159, to which Chl may bind. This residue is homologous to Chl-binding histidines in PsaA (i.e., H199 in the peptide from *T. elongatus*) and PsaB (i.e., H177 in the peptide from *T. elongatus*). Therefore, the new model of IsiA has 13 Chl-binding amino acids (i.e., H46, Q49, E64, H111, H125, H144, H159, H160, H222, H236, H322, H333, and H336). The remaining two Chls, corresponding to Chls in CP43, PsaA, and PsaB, are bound to water and other ligands. Our model of IsiA is shown in Fig. 1A.

Based on our multiple sequence alignment, we discovered another conserved histidine, H84, in IsiA, which is homologous with Q105 of PsaA and H89 of PsaB. Both of these residues are Chl-binding amino acids in PsaA and PsaB, respectively, so it became relevant to find out whether H84 might be a Chl-binding residue. Using PsaA as a template, we inserted a Chl molecule in the corresponding position of IsiA, but it was found to be located too close (5.37 Å) to the Chl binding to H322. The two Chls were also located at a 60° angle in relation to each other and thus not situated in a manner that facilitates efficient energy transfer, although this could, theoretically, be overcome by the close distance. We also compared the modelled structure of IsiA and its CP43 template and found that they are very similar in the region of this H84 residue and that H84 resides in an inflexible loop, which is tucked back into the membrane. Although stacked porphyrin molecules may be found ~6 Å apart, the angle between these molecules in our model would require at least a 2–3 Å relaxation of the surrounding structure. While an extra Chl may be bound to H84, we have discounted it for the present and note that the PsaA structure does not accommodate two Chls here either.

The positions of Mg atoms in Chls associated with IsiA were used to identify the optimal Chl–Chl connections within this molecule. The 15 Chls associated with IsiA form a single network of optimal Chl–Chl connections with a connectivity of 65.7% (Fig. 1B). Some of these Chls are located >25 Å apart, implying that transmission of excitation energy between these Chls must rely on other Chl atoms. Nevertheless, there are no bottlenecks (defined as a Chl associated with only two optimal Chl–Chl connections) in the network because each Chl-bound Mg atom is ≤25 Å apart from those of between four and 13 other Chls. Hence, there are many paths along which excitation energy can move between Chls in IsiA. The new Chl, which binds to H159 in Helix III, is located on the surface of IsiA and its Mg atom is ≤25 Å apart from those of seven other Chls, implying that it is well connected within IsiA and thus could play an important role in transmitting excitation energy between adjacent IsiA monomers and/or the IsiA ring and the PSI trimer.

Two validation methods were used to compare our model of IsiA with the sequence of IsiA. The results obtained using *ValPred*, which resemble those produced by *Harmony*, are shown in Fig. 2. Apart from the N- and C-terminal sequences of the protein, there are 34 residues with negative compatibility scores (i.e., 169–176, 189, 249–250, 288, 292–312, and 323). This implies that our model of IsiA is compatible with a majority of the residues in IsiA. Residues with negative compatibility scores are located mainly in the C-terminal part of Helix III and between Helix V and Helix VI. The above-mentioned Chl-binding residues, including H159, are all located in segments with compatibility scores between 0.203 and 0.622.

The observed diameter of the IsiA subunit protein molecule is 37 Å and, thus, 11 Å less than that calculated for monomers of IsiA in the IsiA–PSI supercomplex (i.e., 48 Å: see Materials and methods). However, a difference of this size was expected because the five carotenoids and 10 of the Chls (i.e., Chls 1, 2, 3, 4, 9, 10, 11, 13, 14, and 15) are located around IsiA, so the estimates of the diameter of IsiA are in fact consistent with each other (the remaining Chls are buried inside this protein: Fig. 1A).

The hydropathy scores for the membrane-spanning helices are all positive (Table 1), implying that these helices are predominantly hydrophobic. However, the standard deviations are large, implying that the six membrane-spanning helices also contain hydrophilic residues. Twelve of the 21 most hydrophilic residues in these helices are Chl-binding amino acids (i.e., H46, Q49, E64, H111, H125, H159, H160, H222, H236, H322, H333 and H336), implying that they are likely to serve critical roles and, therefore, cannot be replaced by hydrophobic amino acids. Six of these Chl-binding residues have their side-chains buried inside the IsiA monomer (i.e., H46, Q49, E64, H111, H322 and H333), implying that their contribution to the surface properties of IsiA may be minimal. Another six of the most hydrophilic amino acids are located at the beginning or end of the helices (i.e., Q67, K151, Q152, E216, D217 and E254), implying that they most likely are found close to one of the two surfaces of the thylakoid membrane.

The spatial distribution of amino acids in the new model of IsiA was examined further, and it was discovered that the membrane-spanning helices may be divided into the following three groups, on the basis of their proximity to one another: Helix I and Helix II in the first group, Helix III and Helix IV in the second group, and Helix V and Helix VI in the third group (Fig. 1A). The helices in each of these groups were furthermore placed at oblique angles in relation to each other and in relation to the thylakoid membrane, implying that the surfaces of adjacent IsiA monomers are unlikely to complement one another unless the adjacent IsiA monomers are situated in the parallel configuration. This, in turn, implies that the anti-parallel model of the IsiA ring (see below) is unlikely to exist.

The numbers of optimal Chl–Chl connections between adjacent IsiA monomers (d_1) and between the IsiA ring and the PSI trimer (d_2) were recorded for 6,969,600 structural configurations of the 18-mer IsiA–PSI supercomplex with 15 Chls in each IsiA monomer. The range of d_2 (from 0 to 51) is wider than that of d_1 (from 2 to 9) (Fig. 3), implying (*i*) that some configurations have a higher energy-transfer potential than others, and (*ii*) that rearranging different subsections of the IsiA–PSI supercomplex has a larger impact on the energy-transfer potential between the IsiA ring and the PSI trimer than on that between adjacent IsiA monomers. The Pareto front in Fig. 3 is composed of four points, two of which (i.e., $(d_1, d_2) = (4, 51)$ and (5, 48)) represent four lumen-model configurations and 57 stroma-model configurations; the remaining two points ($(d_1, d_2) = (8, 39)$ and (9, 36)) represent 65 lumen-model configurations. Each of these 126 configurations has a higher energy-transfer potential than most of the other configurations (i.e., those represented by points on the lower left-hand side of each of the four points on the Pareto front).

The results in Fig. 3 can be used to calculate a joint energy-transfer potential for each of the 6,969,600 configurations. For example, $(d_1, d_2) = (4, 15)$ for the Reference model, so the joint energy-transfer potential for this configuration equals $18 \times 4 + 15 = 87$ (note that this number discounts the remaining optimal Chl–Chl connections, all of which are the same for each of the 6,969,600 configurations). The highest joint energy-transfer potential (198) was found to occur in the 50 lumen-model configurations marked L_{best} in Fig. 3. Each of these 50 configurations has over twice (228%) the joint energy-transfer potential of the Reference model; in fact, the joint energy-transfer potential of the Reference model is lower than those of 3,392,977 (48.7%) other lumen- and stroma-model configurations.

The 50 lumen-model configurations with the highest joint energy-transfer potential can be partitioned into three variants of the IsiA–PSI supercomplex (Table 2). The discriminating factor between these three variants is how far the PSI trimer is rotated counterclockwise in relation to its position in the Reference model (i.e., variant A: 6.0–6.5°; variant B: 9.5–10.0°; variant C: 15.0–16.0°). With respect to the displacement of the IsiA ring and the rotation of the IsiA monomers, the three variants are very similar: the PSI trimer is displaced 11–14 Å downwards in relation to its position in the Reference model whereas the IsiA monomers are rotated 213.5–215.0° counterclockwise in relation to their positions in the Reference model. Although these variants have the same joint energy-transfer potential, they differ with respect to the number of Chls involved in the formation of optimal Chl–Chl connections between the IsiA ring and the PSI monomers:

- Variant A configurations use Chls 1, 9, 12, and 15 from the IsiA monomers and Chls A14, B33, J02, J03, and X01 from the PSI monomers
- Variant B configurations use Chls 1, 6, 9, 12, and 15 from the IsiA monomers and Chls A14, B33, J01, J02, and J03 from the PSI monomers
- Variant C configurations use Chls 1, 6, 9, 12, and 15 from the IsiA monomers and Chls A14, B33, J01, J02, J03, and X01 from the PSI monomers.

The positions of Mg atoms in Chls associated with the IsiA–PSI supercomplex were used to draw partial networks of optimal Chl–Chl connections for the Reference model (Fig. 4A) and for one of the 50 configurations with the highest joint energy-transfer potential (Fig. 4B). A comparison of these two networks shows several differences with potential bearings on the performance of the photosynthetic machinery (Table 3). Compared to the Reference model, the configuration in Fig. 4B has: (*i*) more optimal Chl–Chl connections between adjacent IsiA monomers (d_1), (*ii*) more optimal Chl–Chl connections between the IsiA ring and the PS I trimer (d_2), (*iii*) more Chls involved in forming optimal Chl–Chl connections between neighbouring IsiA monomers, (*iv*) more IsiA-associated Chls involved in forming optimal Chl–Chl connections with the PS I trimer, (*v*) more PSI-associated Chls involved in forming optimal Chl–Chl connections with the IsiA ring, and (*vi*) more IsiA monomers involved in forming optimal Chl–Chl connections with the PS I trimer. Importantly, the new Chl associated with IsiA serves an important role in the optimal configuration but not in the Reference model (Fig. 4).

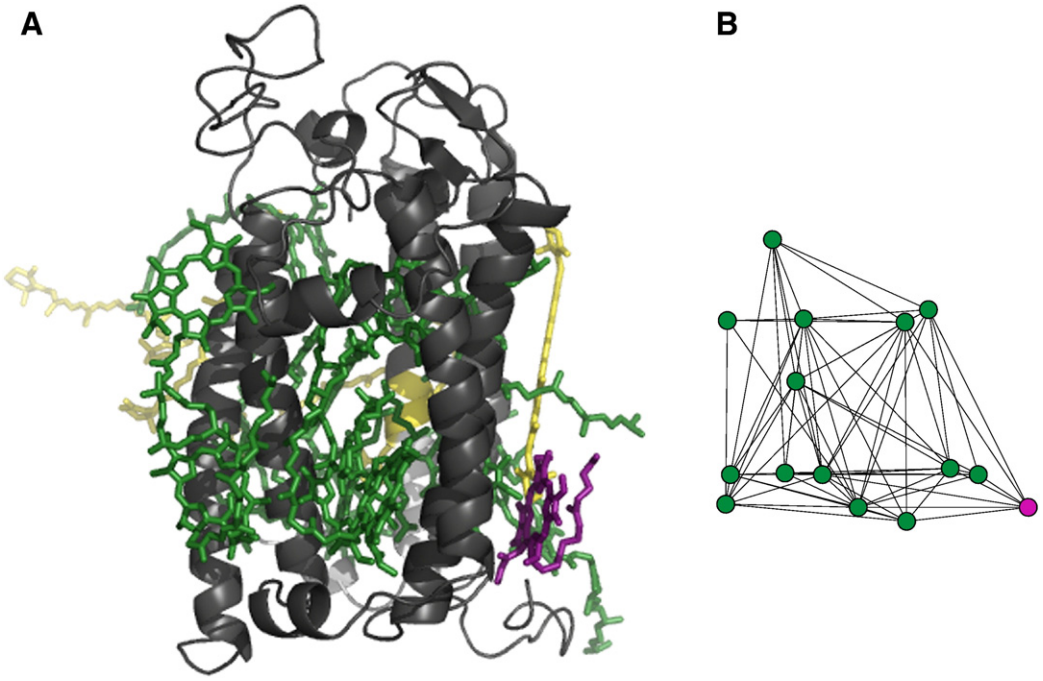

Fig. 1. (A) The new model of IsiA, with its 15 Chls and five carotenoids, which correspond to those of CP43. Helices are in grey, Chls are in green and magenta, and carotenoids are in yellow. The new Chl is in magenta. (B) The network of optimal Chl–Chl connections (i.e., defined as occurring when Chl-bound Mg atoms are ≤25 Å apart), with previously predicted Chls in green and the new Chl in magenta. The figures are drawn to scale and are viewed from the same angle.

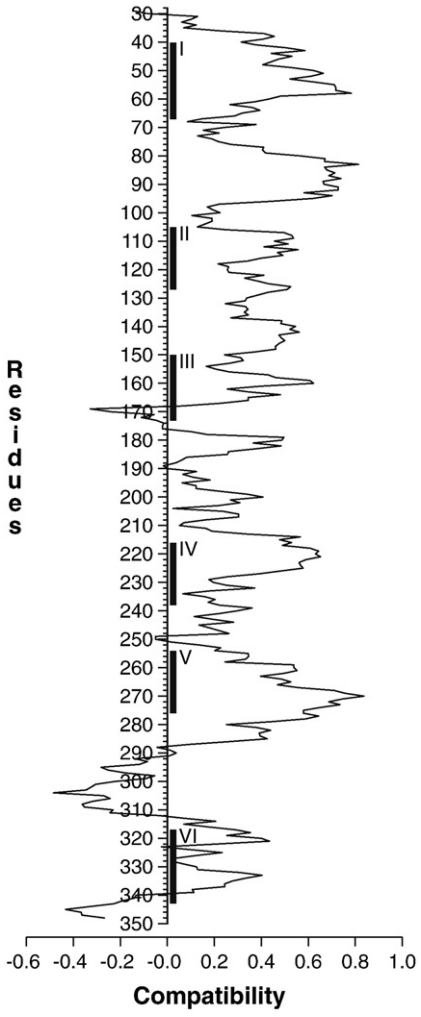

Fig. 2. The smoothed (window size: 10) distribution of compatibility scores for the IsiA model. The compatibility scores and residue numbers are displayed along the *x*- and *y*-axes, respectively (the higher the compatibility score, the more reliable the model prediction is). The black bars highlight residues forming the six membrane-spanning helices.

The positions of Mg atoms in Chls associated with the PSI trimer and PSI monomer were also used to construct networks of optimal Chl–Chl connections. The Chls associated with the PSI monomer form a well-connected network with 12.87% connectivity: the average number of optimal Chl–Chl connections is 12.2 ± 3.87 [SD] and there are no bottlenecks (each Chl-bound Mg atom is ≤ 25 Å apart from between three and 21 other Chl-bound Mg atoms). Similar results were obtained for the PSI trimer (the average number of optimal Chl–Chl connections is 12.3 ± 3.80 [SD] and each Chl-bound Mg atom is ≤ 25 Å apart from between three and 21 other Chl-bound Mg atoms),

Table 1
For each membrane-spanning helix of IsiA, the table shows the relevant residues, the average hydropathy score ($\pm$ the SD), and the most hydrophilic residues (Chl-binding amino acids are in **bold** while residues with a side-chain buried in the monomer of IsiA are in underlined).

Helix	Residues	Hydropathy score	Strongly hydrophilic residues
I	40–67	1.10 ± 2.60	**H46**, **Q49**, **E64**, Q67
II	105–127	1.68 ± 2.44	**H111**, **H125**
III	150–173	1.58 ± 2.94	K151, Q152, **H159**, **H160**
IV	216–238	1.43 ± 3.05	E216, D217, **H222**, **H236**
V	254–276	1.50 ± 2.22	E254
VI	317–343	0.85 ± 2.75	N320, **H322**, Q331, **H333**, **H336**, R339

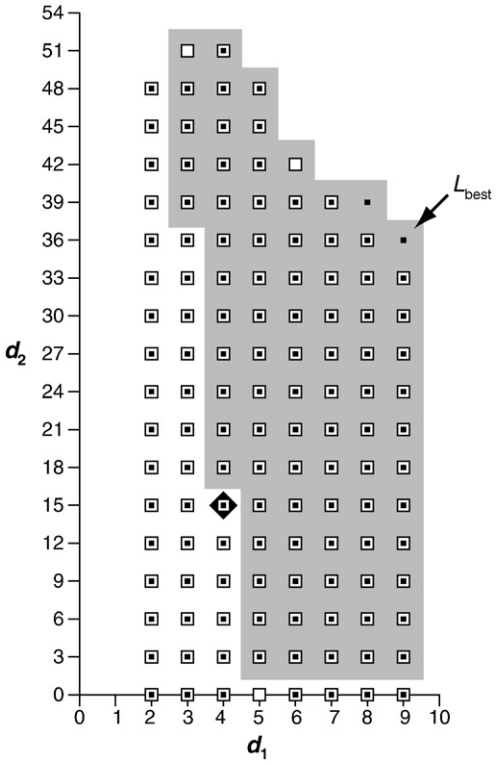

Fig. 3. A Pareto plot of the number of optimal Chl–Chl connections (i.e., defined as occurring when Chl-bound Mg atoms are ≤ 25 Å apart) (*i*) between Chls in adjacent IsiA monomers (d_1), and (*ii*) between Chls in the IsiA ring and in the PS I trimer (d_2). Results for lumen and stroma models are shown using small, black squares and large, white squares, respectively, while the Reference model is highlighted using a black diamond. L_{best} represents 50 optimal structures found among 6,969,600 configurations considered in this study. Points placed on the grey background represent configurations with a joint energy-transfer potential that is higher than that of the Reference model.

Table 2
Three variants of the optimal lumen-model of the IsiA–PSI supercomplex (based on the 50 optimal lumen-model configurations identified in this study). Each variant corresponds to a set of similar configurations, each of which was obtained by rearranging subsections of the Reference model (i.e., that published by Nield et al. [19]).

Variant	PSI trimer		IsiA monomers	Configurations
	Displacement (Å) [a]	Rotation (°) [b]	Rotation (°) [c]	
A	14.0	6.0	215.0	1
–	13.0–13.5	6.5	215.0–214.5	4
–	13.0	6.5	215.0	1
–	12.5	6.5	214.5	1
B	12.5	9.5	213.5–214.0	2
–	12.0	9.5	214.0–215.0	3
–	11.5	9.5	214.5	1
–	13.0	10.0	214.0	1
C	13.5	15.0	213.5	1
–	12.0–13.0	15.0	213.5–214.0	6
–	12.0	15.0	214.5	1
–	14.0	15.5	213.5	1
–	13.5	15.5	213.5–214.0	2
–	11.5–13.0	15.5	213.5–214.5	12
–	11.5–12.0	15.5	215.0	2
–	11.0	15.5	214.5–215.0	2
–	14	16.0	213.5	1
–	12.5–13.5	16.0	213.5–214.0	6
–	12.5–13.0	16.0	214.5	2

[a] The PSI trimer was displaced downwards along its major axis in relation to the IsiA ring.
[b] The PSI trimer was rotated counterclockwise around its own major axis.
[c] The IsiA monomers were rotated counterclockwise around their own major axes.

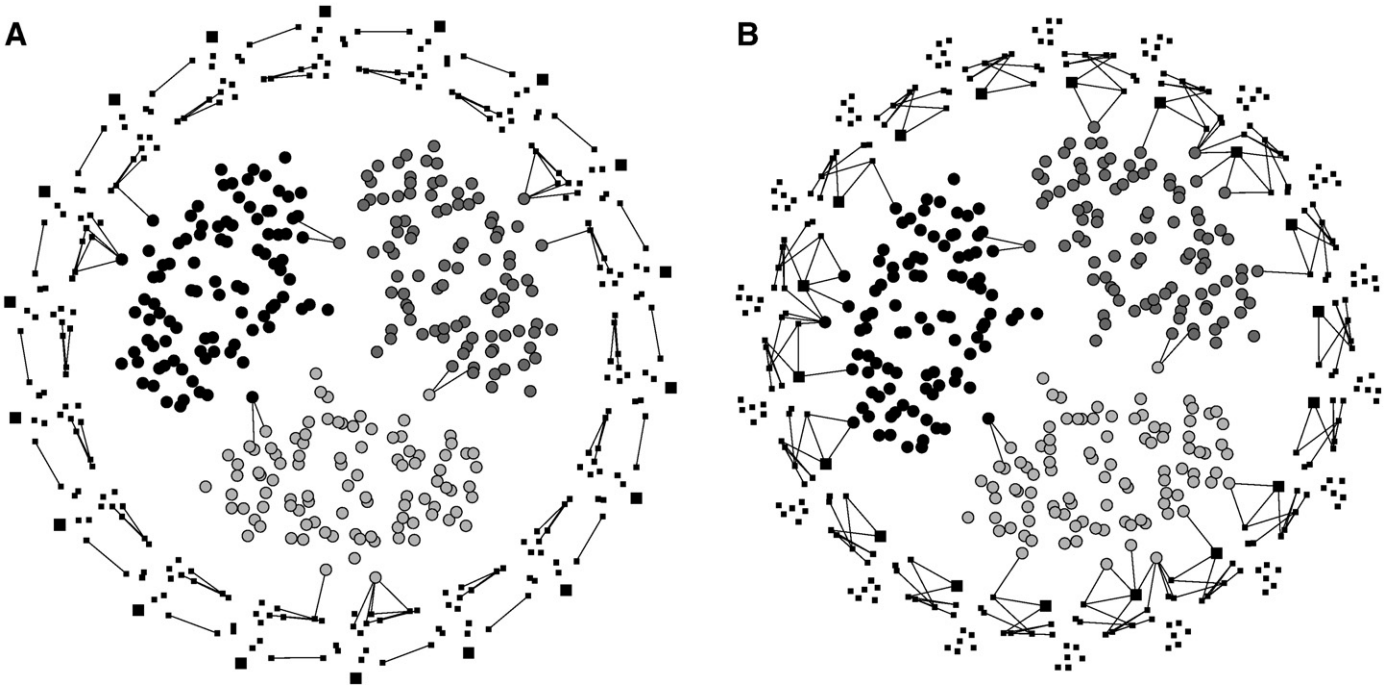

Fig. 4. Comparison of the positions of Mg atoms in Chls associated with the Reference model (A) and one of the 50 optimal lumen-model configurations identified in this study (B). Black squares represent Mg atoms associated with IsiA (large squares represent those associated with the new Chls). Large circles represent Mg atoms associated with the PSI trimer (those with the same hue represent Mg atoms associated the same PSI monomer). Lines represent optimal Chl–Chl connections (i.e., defined as occurring when Chl-bound Mg atoms are ≤25 Å apart) between adjacent Chls in: (*i*) adjacent IsiA monomers, (*ii*) the IsiA ring and PSI trimer, and (*iii*) adjacent PSI monomers. The configuration on the right can be derived from the Reference model with: (*i*) the PSI trimer displaced 13 Å downwards, (*ii*) the PSI trimer rotated 16° counterclockwise, and (*iii*) IsiA monomers rotated 214° counterclockwise.

except that the network's connectivity was 4.28%, due mainly to the much larger dimensions of the PSI trimer. One distinct feature of this network of optimal Chl–Chl connections is the presence of only two such connections between adjacent PSI monomers (Fig. 4). Although the three Chls forming these optimal Chl–Chl connections (i.e., A21, M01, and PG01) are connected to five, nine, and 13 other Chls and, thus, may be considered well-connected, it is also likely that transfer of excitation energy between the PSI monomers may be somewhat restricted. It is also possible that energy pathways are controllable, for example by moving the IsiA ring up or down along its major axis in relation to the PSI trimer.

Table 3
Comparison of the Reference model (i.e., that published by Nield et al. [19]) and one of the 50 optimal lumen-model configurations identified in this study.

Selected Features	Reference model	Optimal model [a]
Optimal Chl–Chl connections between adjacent IsiA monomers (d_1)	4	9
Optimal Chl–Chl connections between the IsiA ring and the PSI trimer (d_2)	15	36
Chls involved in forming optimal Chl–Chl connections between adjacent IsiA monomers [b]	7	8
IsiA-associated Chls involved in forming optimal Chl–Chl connections with the PS I trimer [c]	15	30
PSI-associated Chls involved in forming optimal Chl–Chl connections with the IsiA ring [d]	6	18
IsiA monomers involved in forming optimal Chl–Chl connections with the PSI trimer	6	15

[a] This optimal model corresponds to the Reference model with the (*i*) PSI trimer displaced 13 Å downwards, (*ii*) PSI trimer rotated 16° counterclockwise, and (*iii*) IsiA monomers rotated 214° counterclockwise (i.e., that shown in Fig. 4B).
[b] These connections involve Chls 1, 2, 3, 4, 11, 13, and 14 in the Reference model, and Chls 1, 4, 7, 9, 11, 12, 14, 15 in the optimal model.
[c] These connections involve Chls 2, 3, 8, and 14 in the Reference model, and Chls 1, 6, 9, 12, and 15 in the optimal model.
[d] These connections involve Chls J02 and J03 in the Reference model, and Chls A14, B33, J01, J02, J03 and X01 in the optimal model.

4. Discussion

Cyanobacteria have developed two systems for harvesting light: (*i*) the membrane-extrinsic PBP complex, which harvests light in the green to orange regions of the visible spectrum, and (*ii*) the membrane-intrinsic CBP complex [47], which harvests light in the blue and the red regions of the visible spectrum. The PBP complex requires a high input of nitrogen, while, in low-nitrogen environments, the CBP complex may be switched on by environmental cues, as happens in many cyanobacteria [2], or may operate constitutively, as in *Prochlorococcus marinus* and *Acaryochloris marina* [2]. The CBP complex incorporates IsiA, which is able to form an 18-mer ring around a PSI trimer, the whole forming a disk-like supercomplex that is embedded in the thylakoid membrane. While IsiA may be viewed as having evolved to form an antenna complex that enhances LH for PSI, it has clearly acquired other functions. For example, under intense light, rings of IsiA may be partially formed or they may be empty [29,30]. This strategy may have coevolved to prevent oversupplying the reaction centres (RCs) with excitation energy, which can lead to harmful side reactions and damage of the photosynthetic machinery [30]. In addition, IsiA has been found to associate with PSII and to act in a LH capacity [33], and it is likely that specific forms of IsiA have evolved for this purpose [2].

The compatibility between the inferred three-dimensional structure of IsiA and its amino-acid sequence was used to assess the reliability of the inferred structure. Two programs, *ValPred* and *Harmony*, were chosen for this purpose because they consider the biochemical properties of the amino acids, albeit with differences in how local environments are defined and treated. The results showed that our model is compatible with most parts of the amino-acid

sequence, and that the only dubious parts of our model are the C-terminal part of Helix III and the loop between Helix V and Helix VI (Fig. 2). However, even here the fit between the model and amino-acid sequence was acceptable, and none of the important features, including the Chl-binding amino acids, are associated with these domains.

IsiA is a member of the family of LH antenna proteins that includes CP43, Pcb, CP47, PscA, PdhA, and the N-terminal parts of PsaA and PsaB [23,47]. In a previous study, we found that IsiA must be a relatively recent addition to the LH parts of the RC, the latter having arisen within anoxygenic photosynthetic bacteria at least 3 billion years ago [23]. Previously, Nield et al. [19] published a similar model of IsiA where the number and positions of Chls was based on the crystal structure of CP43. Our analysis incorporated additional information about the positions of Chl-binding amino acids from other homologous proteins (i.e., PsaA and PsaB) and led to the discovery that IsiA may be associated with 15 Chls, which is one more than those already reported by Nield et al. [19]. Our discovery is consistent with that of Murray et al. [48], who found (*i*) that H159 in IsiA from *T. elongatus* is conserved across IsiAs, and (*ii*) that when IsiA was superimposed on the N-terminal segments of PsaA and PsaB from *T. elongatus*, then H199 in PsaA and H177 in PsaB are placed in the same positions as H159 in IsiA. H199 in PsaA and H177 in PsaB are conserved Chl-binding amino acids, so our results strongly support a model of IsiA with 15 Chls. One consequence of associating each IsiA monomer with one more Chl is that the IsiA ring's potential to absorb light is increased by 7%. Another consequence is that energy transfer occurs more efficiently.

Our examination of the amino acids in our model of IsiA showed that the membrane-spanning helices are hydrophobic, implying that these helices are suited for embedment in the thylakoid membrane. However, the helices still contain some hydrophilic residues. At a first glance, the presence of these residues appeared unlikely, but a closer examination disclosed that: (*i*) 12 of the 21 most hydrophilic residues are Chl-binding amino acids and, thus, of great functional significance; (*ii*) six of these residues have hydrophilic side-chains buried inside the core of the IsiA molecule and, thus, are unlikely to render IsiA's surface locally hydrophilic; and (*iii*) six of the residues are located near the thylakoid membrane's surfaces, which is consistent with the idea that IsiA is a membrane-spanning molecule.

Our examination of the membrane-spanning helices was inspired by a desire to determine whether the distribution of helix-forming amino acids would reveal how each IsiA monomer is positioned with respect to: (*i*) the thylakoid membrane, (*ii*) the adjacent IsiA monomers, (*iii*) the PSI trimer, and (*iv*) the thylakoid membrane's surfaces. Our examination showed that hydrophobic residues are relatively evenly distributed among the membrane-spanning helices. Hence, with only this information available we could not determine how the IsiA monomers are situated in the IsiA–PSI supercomplex, implying that other sources of information would be required to determine their relative positions.

Interestingly, the diameter of the IsiA monomer was estimated to be around 37 Å whereas the diameter of the molecule was expected to be 48 Å. However, the estimate of the diameter was based on the helices and their amino acids, and did not take into account the presence of Chls and other ligands. When these were considered along with the important connections of some IsiA monomers to the PsaJ subunit of the PSI monomer, it appears reasonable to assume that the diameter of IsiA is closer to the expected 48 Å.

As there is no known covalent bonding between the IsiA ring and the PSI trimer, other physico-chemical interactions between these components might be important. In order to transfer excitation energy from the Chls in the IsiA ring to the PSI trimer, we hypothesize that ionic bonding and stable, energy-efficient corridors must stabilize the positions of the two components. Assuming that excitation energy moves along hydrophilic corridors in the IsiA–PSI supercomplex [49], the most closely spaced Chls might then act as a bridge, provided they are nested in a hydrophobic environment and the Mg atoms in adjacent Chls are $\leq$25 Å apart [18]. In so doing, the chlorin rings of the Chls would act like pillars of a bridge over water. Whether this hypothesis is correct, however, will require further study, which is beyond the scope of the present paper.

With this idea in mind, *Cartesian* was produced to manipulate and compare a large number of stroma and lumen models of the IsiA–PSI supercomplex. A total of 3,484,800 lumen-model configurations and 3,484,800 stroma-model configurations were generated by: (*i*) moving the PSI trimer along its major axis in steps of 0.5 Å from −30 Å to +30 Å; (*ii*) rotating the PSI trimer around its major axis in steps of 0.5° from 0° to 20°; and (*iii*) simultaneously rotating the IsiA monomers around their own axes in steps of 0.5° from 0° to 360°. For each structural configuration, we assumed that optimal Chl–Chl connections would form when adjacent Chl-bound Mg atoms were $\leq$25 Å (i.e., our study was based on Förster resonance transfer processes, but did not consider excitonic quantum processes) and then recorded the number of optimal Chl–Chl connections between adjacent IsiA monomers and between the IsiA ring and the PSI trimer. Using multi-objective optimization [46], we found 50 lumen-model configurations that were optimal with respect to their joint energy-transfer potential (Fig. 3); all the remaining configurations, including the model published by Nield et al. [19], had lower joint energy-transfer potentials. Interestingly, Nield et al.'s [19] model had a joint energy-transfer potential that was less than 50% of that for the optimal configurations.

A comparison of the above-mentioned 50 optimal configurations showed that these could be further separated into three variants (Table 2). Members of each variant were similar to each other while those of different variants differed in (*i*) how far the PSI trimer was rotated on its major axis in relation to the IsiA ring and (*ii*) how many IsiA- and PSI-associated Chls were involved in the formation of the networks of optimal Chl–Chl connections. The second point is of potential significance because a network in which the critical Chl–Chl connections (i.e., those that enable transfer of excitation energy between IsiA monomers and between the ring of IsiA monomers and the PSI trimer) are formed by a larger number of Chls (in the present case, variant C configurations: Table 2) is less likely to suffer from energy-induced stress if exposed to periods of intense light than a network in which the critical Chl–Chl connections are formed by fewer number of Chls (such as the variant A and B configurations; Table 2).

What would the optimal structure have been if each IsiA monomer were associated with only 14 Chls? We considered this question, and it turned out that the optimal configuration was a lumen model with the: (*i*) PSI trimer displaced 8.5–9.5 Å downwards along its major axis in relation to the IsiA ring, (*ii*) PSI trimer rotated 6.5–7° counter-clockwise around its own major axis, and (*iii*) the IsiA monomers rotated 211° counterclockwise around their own major axes. Although this model has less optimal Chl–Chl connections than the 50 optimal configurations of the IsiA–PSI supercomplex with 15 Chls associated with each IsiA monomer, it still is very similar in design to the latter (Table 2).

A comparison between the Reference model and one of the variant C configurations showed that the latter models are superior with respect to the energy-transfer potential (Figs. 3 and 4). This superiority is due to the fact that the variant C configurations have more optimal Chl–Chl connections, more Chls involved in forming these connections, and more IsiA monomers involved in forming optimal Chl–Chl connections with the PS I trimer (Table 3). The effect of these differences is an increase in the number of paths along which excitation energy can be transferred from Chls in the IsiA ring to the RCs, a reduction of the shortest distance (measured in terms of nodes in the network) between the Chls in the IsiA ring and the RCs, and a lower potential for light-induced stress on the critical Chls (i.e., those

that form the optimal Chl–Chl connections between IsiA monomers and between the IsiA ring and the PSI trimer).

A closer comparison between Nield et al.'s [19] model of the IsiA–PSI supercomplex and the variant C configurations highlights additional details favouring the latter models. It is reasonable to assume that the complex should be efficient under weak as well as strong light. Here, efficiency is considered in the context of two processes: (*i*) the harvesting of sunlight and the transmission of excitation energy to the RCs, and (*ii*) the dissipation of excess energy, which, if it were to reach the RCs, could damage these [50]. During growth under weak light, light-induced stress is unlikely to damage the RCs, so selective advantage must be determined by the efficiency with which energy is harvested and transmitted to the RCs. If the energy can be dissipated on its way to the RCs, then it is reasonable to assume that such a loss is most likely to occur along long paths in the network of optimal Chl–Chl connections. This implies that variant C configurations would be favoured over the Reference model because it only has six IsiA monomers in direct contact with the PSI trimer whereas the variant C configurations have 15 (Table 3). On the other hand, during growth under intense light, light-induced stress may damage the RCs, so selective advantage must be determined not only by the efficiency with which energy is harvested and transmitted to the RCs but also by its ability to dissipate excess energy from the RCs. If energy needs to be transferred away from the RCs to avoid damage, then it is desirable to transfer it from the PSI trimer to the IsiA ring. This implies, yet again, that the variant C configurations would be favoured over the Reference model because the variant C configurations have 36 optimal Chl–Chl connections between the PSI trimer with the IsiA ring whereas the Reference model has 15 (Table 3). In summary, we have identified models of the IsiA–PSI supercomplex that are superior under low- and high-light conditions to the model published by Nield et al. [19]. It is plausible that one of the variant C configurations may be real but far more data, preferentially a high-resolution crystal structure of the IsiA–PSI supercomplex, will be needed to answer this question.

Even when the latter data become available, there will be many unanswered questions to address. It is plausible that the IsiA–PSI supercomplex may vary across species, implying that what is an optimal configuration for one species might not be so for another species. It is also plausible that the symmetry of the IsiA ring assumed by us is unrealistic — variations might occur in the position and orientation of the IsiA monomers, leading to structures with a highly asymmetric distribution of optimal Chl–Chl connections. Given a good high-resolution crystal structure of the IsiA–PSI supercomplex, it will be particularly important repeat Sener et al.'s [51] study to gain a better understanding of energy transfer within this complex. Likewise, it might be useful to examine the network of optimal Chl–Chl connections using network statistics, such as path length, connectivity, etc.

Acknowledgements

The authors wish to thank Professors DS Bendall (University of Cambridge) and H Scheer (Ludwig-Maximilians-Universität) for constructive advice. The authors also wish to thank Dr DR Lovell (CSIRO), Dr C Jackson (CSIRO), and two anonymous reviews for their encouraging feedback. MC, AWDL, and LSJ gratefully acknowledge financial support from the Australian Research Council.

References

[1] A.W.D. Larkum, Light-harvesting systems in algae, Kluwer Academic, Dordrecht, 2003.
[2] M. Chen, T.S. Bibby, Photosynthetic apparatus of antenna-reaction centres supercomplexes in oxyphotobacteria: insight through significance of Pcb/IsiA Proteins, Photosynth. Res. 86 (2005) 165–173.
[3] H.C. Riethman, L.A. Sherman, Purification and characterization of an iron stress-induced chlorophyll-protein from the cyanobacterium Anacystis nidulans R2, Biochim. Biophys. Acta 935 (1988) 141–151.
[4] K.N. Ferreira, N.A. Straus, Iron deprivation in cyanobacteria, J. Appl. Phycol. 6 (1994) 199–210.
[5] N. Yousef, E.K. Pistorius, K.P. Michel, Comparative analysis of IdiA and IsiA transcription under iron starvation and oxidative stree in *Synechococcus elongatus* PCC 7942 wild-type and selected mutants, Arch. Microbiol. 180 (2003) 471–483.
[6] K.P. Michel, E.K. Pistorius, Adaptation of the photosynthetic electron transport chain in cyanobacteria to iron deficiency: the function of IdiA and IsiA, Physiol. Plant. 120 (2004) 36–50.
[7] M. Havaux, G. Guedeney, M. Hagemann, N. Yeremenko, H.C.P. Matthijs, R. Jeanjean, The chlorophyll-binding protein IsiA is inducible by high light and protects the cyanobacterium Synechocystis PCC6803 from photooxidative stress, FEBS Lett. 579 (2005) 2289–2293.
[8] K. Kojima, T. Suzuki-Maenaka, T. Kikuchi, H. Nakamoto, Roles of the cyanobacterial *isiABC* operon in protection from oxidative and heat stresses, Physiol. Plant. 128 (2006) 507–519.
[9] I. Ardelean, H.C. Matthijs, M. Havaux, F. Joset, R. Jeanjean, Unexpected changes in photosystem I function in a cytochrome *c*6-deficient mutant of the cyanobacterium Synechocystis PCC 6803, FEMS Microbiol. Lett. 213 (2002) 113–119.
[10] R. Jeanjean, E. Zuther, N. Yeremenko, M. Havaux, H.C.P. Mathiijs, M. Hagemann, A photosystem I psaFJ-null mutant of the cyanobacterium Synechocystis PCC 6803 expresses the isiAB operon under iron replete conditions, FEBS Lett. 549 (2003) 52–56.
[11] A.K. Singh, L.A. Sherman, Iron-independent dynamics of IsiA production during the transition to stationary phase in the cyanobacterium *Synechocystis* sp. PCC 6803, FEBS Lett. 256 (2006) 159–164.
[12] U. Dühring, I.M. Axmann, W.R. Hess, A. Wilde, An internal antisense RNA regulates expression of the photosynthesis gene isiA, Proc. Natl. Acad. Sci. U. S. A. 103 (2006) 7054–7058.
[13] T.S. Bibby, I. Mary, J. Nield, F. Partensky, J. Barber, Low-light-adapted prochlorococcus species possess specific antennae for each photosystem, Nature 424 (2003) 1051–1054.
[14] T.S. Bibby, J. Nield, J. Barber, A photosystem II-like protein, induced under iron-stress, forms an antenna ring around the photosystem I trimer in cyanobacteria, Nature 412 (2001) 743–745.
[15] E.J. Boekema, A. Hifney, A.E. Yakushevska, M. Piotrowski, W. Keegstra, S. Berry, K.P. Michel, E.K. Pistorius, J. Kruip, A giant chlorophyll–protein complex induced by iron deficiency in cyanobacteria, Nature 412 (2001) 745–748.
[16] T.S. Bibby, J. Nield, J. Barber, Three-dimensional model and characterization of the iron stress-induced CP43′-photosystem I supercomplex isolated from the cyanobacterium Synechocystis PCC 6803, J. Biol. Chem. 276 (2001) 43246–43252.
[17] E.G. Andrizhiyevskaya, T.M.E. Schwabe, M. Germano, S. D'Haene, J. Kruip, R. Van Grondelle, J.P. Dekker, Spectroscopic properties of PSI–IsiA supercomplexes from the cyanobacterium *Synechococcus* PCC 7942, Biochim. Biophys. Acta 1556 (2002) 265–272.
[18] A.N. Melkozernov, S. Lin, T.S. Bibby, J. Barber, R.E. Blankenship, Time-resolved absorption and emission show that the CP43′ antenna ring of iron-stressed Synechocystis sp. PCC6803 is efficiently coupled to the photosystem I reaction center core, Biochemistry 42 (2003) 3893–3903.
[19] J. Nield, E.P. Morris, T.S. Bibby, J. Barber, Structural analysis of the photosystem I supercomplex of cyanobacteria induced by iron deficiency, Biochemistry 42 (2003) 3180–3188.
[20] P. Jordan, P. Fromme, H.T. Witt, O. Klukas, W. Saenger, N. Kraub, Three-dimensional structure of cyanobacterial photosystem I at 2.5 Å resolution, Nature 411 (2001) 909–917.
[21] A. Zouni, H.T. Witt, J. Kern, P. Fromme, N. Krauss, W. Saenger, P. Orth, Crystal structure of photosystem II from *Synechococcus elongatus* at 3.8 Å resolution, Nature 409 (2001) 739–743.
[22] J. La Roche, G.W.M. Van der Staay, F. Partensky, A. Ducret, R. Aebersold, R. Li, S.S. Golden, R.G. Hiller, P.M. Wrench, A.W.D. Larkum, B.R. Green, Independent evolution of the prochlorophyte and green plant chlorophyll a/b light-harvesting proteins, Proc. Natl. Acad. Sci. U. S. A. 93 (1996) 15244–15248.
[23] Y. Zhang, M. Chen, B.B. Zhou, L.S. Jermiin, A.W.D. Larkum, Evolution of the inner light-harvesting antenna protein family of cyanobacteria, Algae and plants, J. Mol. Evol. 64 (2007) 321–331.
[24] N. Kamiya, J.-R. Shen, Crystal structure of oxygen-evolving photosystem II from *Thermosynechococcus vulcanus* at 3.7 Å resolution, Proc. Natl. Acad. Sci. U. S. A. 100 (2003) 98–103.
[25] K.N. Ferreira, T.M. Iverson, K. Maghlaoui, J. Barber, S. Iwata, Architecture of the photosyntheic oxygen-evolving center, Science 303 (2004) 1831–1833.
[26] J. Biesiadka, B. Loll, J. Kern, K.-D. Irrgang, A. Zouni, Crystal structure of cyanobacterial photosystem II at 3.2 Å resolution: a closer look at the Mn-cluster, Phys. Chem. Chem. Phys. 6 (2004) 4733–4736.
[27] R. Kouril, N. Yeremenko, S. D'Haene, A.E. Yakushevska, W. Keegstra, H.C.P. Matthijs, J.P. Dekker, E.J. Boekema, Photosystem I trimers from *Synechocystis* PCC6803 lacking the PsaF and PsaJ subunits bind an IsiA ring of 17 units, Biochim. Biophys. Acta 1607 (2003) 1–4.
[28] R. Kouril, A.A. Arteni, J. Lax, N. Yeremenko, S. D'Haene, M. Rogner, H.C.P. Matthijs, J.P. Dekker, E.J. Boekema, Structure and function role of supercomplexes of IsiA and Photosystem I in cyanobacterial photosynthesis, FEBS Lett. 579 (2005) 3253–3257.
[29] C.L. Aspinwall, J. Duncan, T. Bibby, C.W. Mullineaux, J. Barber, The trimeric organisation of photosystem I is not necessary for the iron-stress induced CP43′ to functionally associate with this reaction centre, FEBS Lett. 574 (2004) 126–130.

[30] N. Yeremenko, R. Kouril, J.A. Ihalainen, S. D'Haene, N. van Oosterwijk, E.G. Andrizhiyevskaya, W. Keegstra, H.L. Dekker, M. Hagemann, E.J. Boekema, H.C.P. Matthijs, J.P. Dekker, Supramolecular organization and dual function of the IsiA chlorophyll-binding protein in cyanobacteria, Biochemistry 43 (2004) 10308–10313.
[31] A. Wilson, C. Boulay, A. Wilde, C.A. Kerfeld, D. Kirilovsky, Light-induced energy dissipation in iron-starved cyanobacteria: roles of OCP and IsiA proteins, Plant Cell 19 (2007) 656–672.
[32] J.C. Cadoret, R. Demouliere, J. Lavaud, H.J. Van Gorkom, J. Houmard, A.L. Etienne, Dissipation of excess energy triggered by blue light in cyanabacteria with CP43′ (isiA), Biochim. Biophys. Acta 1659 (2004) 100–104.
[33] M. Sarcina, C. Mullineaux, Mobility of the isiA chlorophyll-binding protein in cyanobacterial thylakoid membranes, J. Biol. Chem. 279 (2004) 36514–36518.
[34] B. Loll, J. Kern, W. Saenger, A. Zouni, J. Biesiadka, Towards complete cofactor arrangement in the 3.0 Å resolution structure of photosystem II, Nature 438 (2005) 1040–1044.
[35] N. Guex, M.C. Peitsch, SWISS-MODEL and the Swiss-PdbViewer: an environment for comparative protein modeling, Electrophoresis 18 (1997) 2714–2723.
[36] H.M. Berman, J. Westbrook, Z. Feng, G. Gilliland, T.N. Bhat, H. Weissig, I.N. Shindyalov, P.E. Bourne, The protein data bank, Nucleic Acids Res. 28 (2000) 235–242.
[37] S. Dastmalchi, M.B. Morris, W.B. Church, Modeling of the structural features of integral-membrane proteins using reverse-environment prediction of integral membrane protein structure (REPIMPS), Protein Sci. 10 (2001) 1529–1538.
[38] G. Pugalenthi, K. Shameer, N. Srinivasan, R. Sowdhamini, Harmony: a server for the assessment of protein structures, Nucleic Acids Res. 34 (2006) W231–W234.
[39] J. Kyte, R.F. Doolittle, A simple method for displaying the hydropathic character of a protein, J. Mol. Biol. 157 (1982) 105–132.
[40] Y. Nakamura, T. Kaneko, S. Sato, M. Ikeuchi, H. Katoh, S. Sasamoto, A. Watanabe, M. Iriguchi, K. Kawashima, T. Kimura, Y. Kishida, C. Kiyokawa, M. Kohara, M. Matsumoto, A. Matsuno, N. Nakazaki, S. Shimpo, M. Sugimoto, C. Takeuchi, M. Yamada, S. Tabata, Complete genome structure of the thermophilic cyanobacterium *Thermosynechococcus elongatus* BP-1, DNA Res. 9 (2002) 123–130.
[41] T.H. Förster, Energy transport and fluorescence, Naturwissenschaften 33 (1946) 166–175.
[42] K.J. Riley, V. Zazubovich, R. Jankowiak, Frequency-domain spectroscopic study of the PS I-CP43′ supercomplex from the cyanobacterium *Synechocystis* PCC6803 grown under Iron Stress Conditions, J. Phys. Chem. B. 110 (2006) 22436–22446.
[43] A.N. Melkozernov, J. Barber, R.E. Blankenship, Light harvesting in photosystem I supercomplexes, Biochemistry 45 (2006) 331–345.
[44] A.N. Melkozernov, R.E. Blankenship, Structural and functional organization of the peripherial light-harvesting system in photosystem I, Photosynth. Res. 85 (2005) 33–50.
[45] W.L. Delano, The PyMOL molecular graphics system, Delano scientific, Palo Alto, CA, USA, 2002.
[46] K. Deb, Multi-objective Optimization using Evolutionary Algorithms, John Wiley and Sons, 2001.
[47] M. Chen, Y. Zhang, R.E. Blankenship, Nomenclature for membrane-bound light-harvesting complexes of cyanobacteria, Photosynth. Res. 95 (2008) 147–154.
[48] J.W. Murray, J. Duncan, J. Barber, CP43-like chlorophyll binding proteins: structural and evolutionary implications, Trends Plant Sci. 11 (2006) 152–158.
[49] A. Ben-Shem, F. Frolow, N. Nelson, Crystal structure of plant photosystem I, Nature 426 (2003) 630–635.
[50] J.M. Anderson, W.S. Chow, Y.-I. Park, The grand design of photosynthesis: acclimation of the photosynthetic apparatus to environmental cues, Photosynth. Res. 46 (1995) 129–139.
[51] M.K. Sener, S. Pak, D. Lu, A. Damjanovic, T. Ritz, P. Fromme, K. Schulten, Excitation migration in trimeric cyanobacterial photosystem I, J. Chem. Phys. 120 (2004) 11183–11195.